

Large-area display textiles integrated with functional systems

<https://doi.org/10.1038/s41586-021-03295-8>

Received: 9 August 2020

Accepted: 26 January 2021

Published online: 10 March 2021

 Check for updates

Xiang Shi^{1,2,3,11}, Yong Zuo^{1,2,3,11}, Peng Zhai^{4,11}, Jiahao Shen⁵, Yangyiwei Yang⁶, Zhen Gao^{1,2,3}, Meng Liao^{1,2,3}, Jingxia Wu^{1,2,3}, Jiawei Wang^{1,2,3}, Xiaojie Xu^{1,2,3}, Qi Tong⁵, Bo Zhang^{1,2,3}, Bingjie Wang^{1,2,3}, Xuemei Sun^{1,2,3}, Lihua Zhang^{4,7}, Qibing Pei⁸, Dayong Jin^{9,10}, Peining Chen^{1,2,3}✉ & Huisheng Peng^{1,2,3}✉

Displays are basic building blocks of modern electronics^{1,2}. Integrating displays into textiles offers exciting opportunities for smart electronic textiles—the ultimate goal of wearable technology, poised to change the way in which we interact with electronic devices^{3–6}. Display textiles serve to bridge human–machine interactions^{7–9}, offering, for instance, a real-time communication tool for individuals with voice or speech difficulties. Electronic textiles capable of communicating¹⁰, sensing^{11,12} and supplying electricity^{13,14} have been reported previously. However, textiles with functional, large-area displays have not yet been achieved, because it is challenging to obtain small illuminating units that are both durable and easy to assemble over a wide area. Here we report a 6-metre-long, 25-centimetre-wide display textile containing 5×10^5 electroluminescent units spaced approximately 800 micrometres apart. Weaving conductive weft and luminescent warp fibres forms micrometre-scale electroluminescent units at the weft–warp contact points. The brightness between electroluminescent units deviates by less than 8 per cent and remains stable even when the textile is bent, stretched or pressed. Our display textile is flexible and breathable and withstands repeated machine-washing, making it suitable for practical applications. We show that an integrated textile system consisting of display, keyboard and power supply can serve as a communication tool, demonstrating the system's potential within the 'internet of things' in various areas, including healthcare. Our approach unifies the fabrication and function of electronic devices with textiles, and we expect that woven-fibre materials will shape the next generation of electronics.

Display devices have evolved from rigid panels to flexible thin films¹⁵. However, the configuration and fabrication of electronic textiles are different from conventional film devices, such as organic light-emitting diodes (OLEDs) that are currently used to construct flexible displays. On one hand, textiles are woven from fibres, forming rough and porous structures that can deform and fit the contours of the human body^{16,17}. OLEDs, on the other hand, are made by depositing multiple layers of semiconducting organic thin films between cathode and anode electrodes that are placed on planar substrates such as glass or plastic¹⁸. Therefore, when attached onto the rough and deformable surfaces of textiles, these film devices often perform poorly or fail over time¹⁹. Depositing organic thin films on fibres that are suitable for weaving into flexible display textiles is also very difficult because these thin films are too fragile to withstand the chafing during weaving. The evaporation

method used to make OLEDs is not amenable to large-scale fabrication of fibre electrodes. More importantly, because light emission in OLEDs depends on carrier injection and transport between the anode and cathode^{20,21}, weaving warps and wefts cannot provide sufficient high-quality ohmic contact between the electrodes and semiconducting layers for illumination. Although fibre light-emitting devices—such as optical fibres²², polymer light-emitting electrochemical cell fibres²³ and a.c. electroluminescence fibres^{24–26} (Extended Data Table 1)—can be woven into lighting textiles, they generally show pre-designed patterns. The inability to dynamically control the pixels individually in real time according to input digital signals—as in standard display applications such as computers and mobile phones—is a considerable limitation.

In our study, we used electric field-driven devices based on ZnS phosphor to weave a display textile. Unlike OLED devices, ZnS phosphor

¹State Key Laboratory of Molecular Engineering of Polymers, Fudan University, Shanghai, China. ²Department of Macromolecular Science, Fudan University, Shanghai, China. ³Laboratory of Advanced Materials, Fudan University, Shanghai, China. ⁴The Institute of AI and Robotics, Fudan University, Shanghai, China. ⁵Department of Aeronautics and Astronautics, Fudan University, Shanghai, China. ⁶Mechanics of Functional Materials Division, Institute of Materials Science, Technische Universität Darmstadt, Darmstadt, Germany. ⁷Ji Hua Laboratory, Foshan, China. ⁸Department of Materials Science and Engineering, Henry Samueli School of Engineering and Applied Science, University of California, Los Angeles, Los Angeles, CA, USA. ⁹Institute for Biomedical Materials & Devices (IBMD), Faculty of Science, University of Technology Sydney, Sydney, New South Wales, Australia. ¹⁰Department of Biomedical Engineering, UTS-SUStech Joint Research Centre for Biomedical Materials and Devices, Southern University of Science and Technology, Shenzhen, Guangdong, China. ¹¹These authors contributed equally: Xiang Shi, Yong Zuo, Peng Zhai. ✉e-mail: peiningc@fudan.edu.cn; penghs@fudan.edu.cn

dispersed in an insulating polymer matrix is activated by alternating an electric field across a polymer matrix²⁷. Such electric field-driven devices require only spatial contacts between wefts and warps to illuminate^{28,29}, making them intrinsically durable and suitable for large-scale production. We prepared transparent (over 90% transmittance) conductive weft fibres by melt-spinning ionic-liquid-doped polyurethane gel (Extended Data Fig. 1a–c), and luminescent warp fibres by coating commercially available ZnS phosphor on silver-plated conductive yarn (Extended Data Fig. 1d–f). This solution-based coating is a simple way to obtain continuous lengths of luminescent warp fibres. We chose polyurethane as polymer matrix because it is durable to friction, compression and bending during weaving. To ensure uniform coating of ZnS, we dip-coated the conductive yarn in ZnS phosphor slurry and passed it through a home-made scraping micro-pinhole before drying (Extended Data Fig. 2a). The micro-pinhole smoothed the coating along the longitudinal and circumferential directions (Extended Data Fig. 2b, c). Different diameters of the micro-pinhole were used to tune the thickness of the ZnS phosphor layer. We used an optimized thickness of approximately 70 μm in our experiments unless specified otherwise. To evaluate the uniformity of the luminescent coating, we placed a 100-m-long luminescent warp into salt water and applied an alternating voltage between them (Extended Data Fig. 2d). The luminescence remained stable even when twisted (Extended Data Fig. 2e). For a 30-m-long fibre, the luminescence intensity varied by less than 10% (Extended Data Fig. 2f, g). The intensity along the circumference at different locations of the fibre was almost identical and was independent of observation angle (Extended Data Fig. 2h). Fibres with an uneven ZnS phosphor coating (Extended Data Fig. 2i) showed uneven brightness and failure in some electroluminescent units (EL units; Extended Data Fig. 2j, k), indicating that the light emission requires a uniform luminescent coating.

When the conductive weft and luminescent warp fibres are woven with cotton yarn using an industrial rapier loom, each interlaced weft and warp forms an EL unit (Fig. 1a, Extended Data Fig. 1h, i). Synthetic fibre materials such as nylon and polyester fibres could also be co-woven with conductive weft and luminescent warp fibres for various applications (Extended Data Fig. 1j, k). Using this method, we produced a 6 m \times 25 cm (length \times width) large-area display textile containing approximately 5×10^5 EL units (Fig. 1b, Supplementary Video 1). The relative deviations of emission intensity of the 600 EL units varied by <8% (Fig. 1c, d). Such small differences in intensity indicate that these fibres are well suited for making large-area display textiles at scale. After 1,000 cycles of bending (Fig. 1e), stretching (Fig. 1f) and pressing (Fig. 1g), the intensity for a vast majority of the EL units remained stable (with <10% variation). Moreover, the intensity of the majority of the EL units varied by <15% even after repeated folding along different directions (Extended Data Fig. 3a–h), and the intensity of the EL units at the folding line remained stable over 10,000 cycles of folding in each folding direction (Extended Data Fig. 3i–l), indicating superior durability over traditional film displays. We also obtained colourful textiles (Fig. 1h) with uniformly spaced EL units (Fig. 1i) by doping different elements such as copper and manganese into the ZnS phosphor³⁰. Because the fibres are woven, the density of the EL units can be easily tuned by adjusting the weaving parameters to change the distance between the weft–warp contact points (Fig. 1j). The narrowest spacing we achieved here is approximately 800 μm . Based on the project area of the textile, we obtained an average luminance of 122 cd m^{-2} (Extended Data Fig. 4a), a value comparable to commercial planar displays (100–300 cd m^{-2}).

To turn on the EL units, we applied an alternating voltage to the luminescent warps and conductive wefts, generating a low, microampere current to power the units (Fig. 2a). Electric field-induced excitation of the luminescent centre and recombination of electron–hole pairs³¹ results in light emission from the ZnS phosphor at the weft–warp contact area. By varying the applied electricity, we could accurately tune the luminance of the EL unit. The luminance intensity increased

with voltage and frequency (Extended Data Fig. 4b, c). A luminance of 115.1 cd m^{-2} was obtained at a voltage of 3.7 V μm^{-1} and frequency of 2,000 Hz, with a current density of 1.8 mA cm^{-2} and power consumption of 363.1 μW (Extended Data Fig. 4d, e). At such a low power consumption, heating was negligible (Extended Data Fig. 4g, h), which is crucial for large-area clothing applications. The driving voltage for the display textile could be reduced to less than 36 V by decreasing the thickness of the luminescent layer (Extended Data Fig. 4i). Coating the conductive wefts and luminescent warps with a layer of transparent insulating polymer can further ensure the safety of these devices.

Because light emission also depends on how uniform the electric field is at the curved contact area between the luminescent warp and conductive weft, we used a finite-element method to simulate the electric field distribution in the luminescent layer (Fig. 2b). We found that the distribution at the curved contact under an applied voltage was as uniform as a planar electroluminescent device (Fig. 2b, Extended Data Fig. 5a–f) and remained uniform even when the contact area was changed (Fig. 2c, Extended Data Fig. 5g). We attribute this electric field homogeneity to the elastic conductive weft that readily deforms to fit the curved and less elastic surface of the luminescent warp (Extended Data Fig. 1g, h). Light emission occurred even when the conductive weft was leaned, twisted and knotted with the luminescent warp (Fig. 2d, Supplementary Video 2). Electroluminescence mapping images show that electroluminescence intensities and EL unit areas remained nearly unchanged when the transparent conductive weft was moved along the luminescent warp (Fig. 2e), rotated around the contacting point (Fig. 2f), and bent with increasing bending angles (Fig. 2g). As the conductive weft slid along the luminescent warp in increments of 0.5 mm, the luminance varied by less than 2.2% for a distance of up to 3 mm (Fig. 2h). When the transparent weft rotated by $\pm 15^\circ$ from the position perpendicular to the luminescent warp, the electroluminescence intensity fluctuated by less than 2.6% (Fig. 2i). Furthermore, owing to the elasticity of the transparent weft, the luminescence recovered instantly and remained stable over 100 cycles of pressing and releasing the EL unit (Fig. 2j). Bending the transparent weft or luminescent warp up to 1.8 mm from its original state also resulted in fluctuations of less than 2.3% (Fig. 2k, l). Because the fibre is cylindrical, the EL intensity was well maintained when the transparent weft was rolled around its central axis (Extended Data Fig. 6a). The inert and non-volatile nature of the ionic liquid³² in the transparent conductive weft also contributed to the electrical and optical stability of the EL unit (Extended Data Fig. 6b, c). Leaving the textile in the open air for one month did not show any obvious decrease in luminance (Extended Data Fig. 6d). Further, the brightness of the EL units endured 100 cycles of accelerated washing and drying (Extended Data Fig. 6e–h).

To show our weaving strategy is general, we used it to produce other electronic functions within the textile (for example, keyboard and power supply). To create a textile keyboard that functions through dynamic contact, we wove low-resistance warp (silver-plated yarn) with high-resistance weft (carbon fibre) to form a 4 \times 4 keyboard (Extended Data Fig. 7a), where the intersections of the weft and warp form the keys (Extended Data Fig. 7b, c). For the power supply, we wove photoanode wefts with silver-plated conductive yarns to harvest solar energy (Extended Data Fig. 8a–f). The photoanode weft is a titanium (Ti) wire coated with a photoactive layer composed of titanium dioxide (TiO₂) nanotubes as the electron transport layer, dye molecules as the sensitizer and copper iodide (CuI) as the solid electrolyte. Integrating these warps and wefts with battery fibres assembled from flexible MnO₂-coated carbon nanotube fibre (cathode), zinc wire (anode) and ZnSO₄ gel electrolyte, we realized both power generation and storage in the textile (Extended Data Fig. 8j–l). With a display, keyboard and power supply, we can design various multifunctional integrated textile systems for different applications (Fig. 3a, Extended Data Fig. 9).

As a proof-of-concept, we connected the woven display, keyboard and power supply to a display driver, microcontroller and Bluetooth

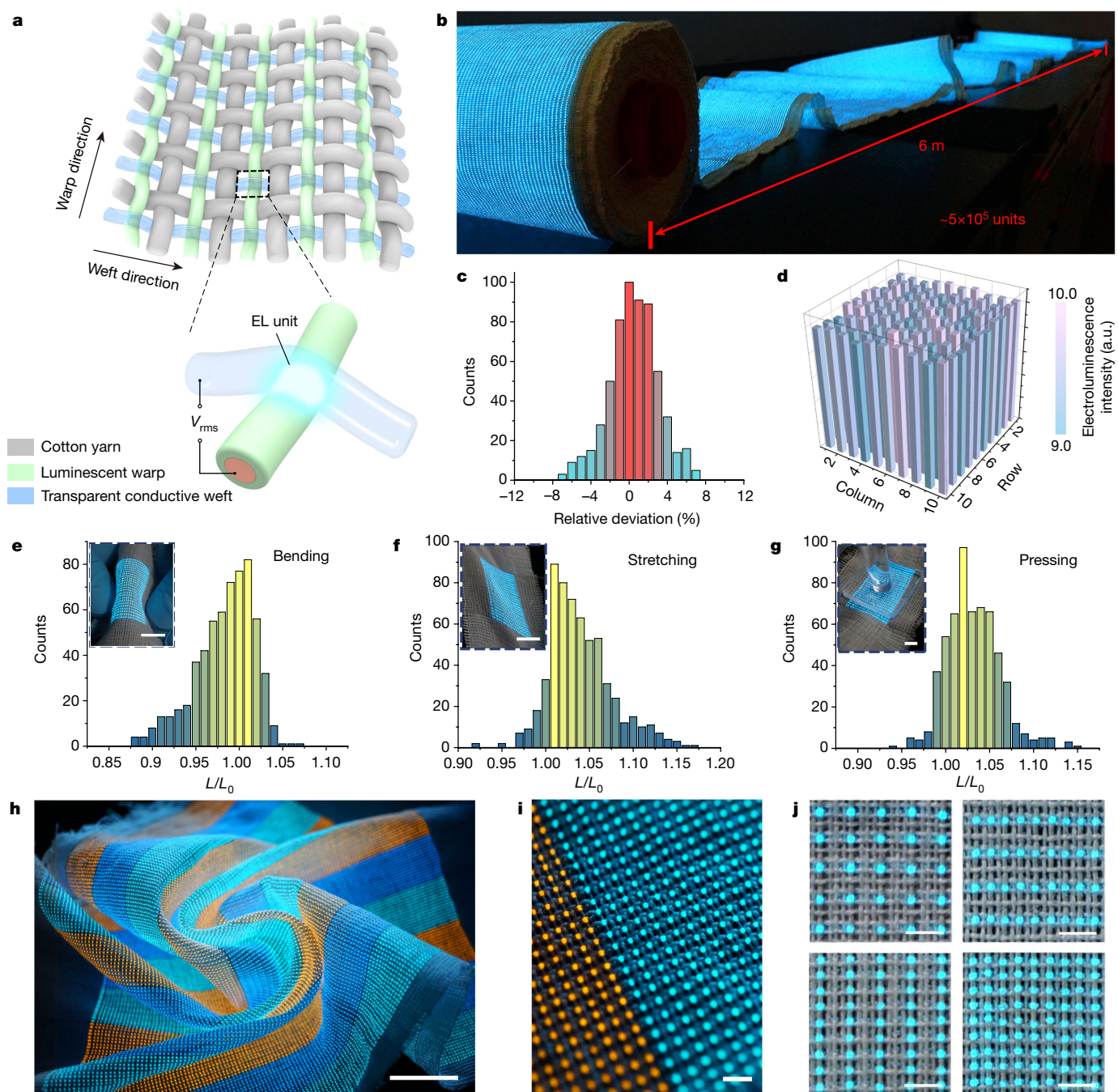


Fig. 1 | Structure and electroluminescence performance of the display textile. **a**, Schematic showing the weave diagram of the display textile. Each contacting luminescent warp and transparent conductive weft forms an EL unit (inset). An applied alternating voltage (V_{rms}) turns on the EL units. **b**, Photograph of a 6-m-long display textile consisting of approximately 5×10^5 EL units. **c**, Statistical distribution showing the relative deviation in emission intensity for 600 EL units. The relative deviation is defined as the deviation of luminance for a single EL unit from the average value. **d**, Emission intensities of a 10×10 EL unit array are uniform (<10% difference in intensity among the units). **e–g**, Statistical distribution showing minor (<10%) variations in

luminance for 600 EL units after 1,000 cycles of bending (**e**), stretching (**f**) and pressing (**g**). Insets, photographs of tested samples. Scale bars, 1 cm. **h**, Photograph of a functional multicolour display textile under complex deformations, including bending and twisting. Blue and orange are achieved by doping ZnS with copper and manganese, respectively. Scale bar, 2 cm. **i**, Magnified photograph of the multicolour display textile from **h** shows that the EL units are uniformly spaced at a distance of $\sim 800 \mu\text{m}$. Scale bar, 2 mm. **j**, Photographs of EL units spaced at different distances, obtained by changing the weave parameters. Scale bars, 2 mm. a.u., arbitrary units.

module (Fig. 3b) and used the integrated textile system as an interactive navigation display (Fig. 3c). Through the Bluetooth module, the user's real-time location in a T-junction, obtained from a smartphone, was transferred to the textile (Fig. 3d). To output the image on the display textile, electrical signals from the driver circuit are scanned row by row onto the array of EL units (Fig. 3e, Supplementary Video 3).

Our integrated textile system can also function as a communication tool, where information is input and displayed on the textile (Fig. 3f, Supplementary Video 3). We demonstrate this using the numbers 1, 2 and 3. Each number is assigned to a key and the microcontroller is programmed to output the number when the corresponding key is pushed (Fig. 3g). With the Bluetooth module, messages can also be

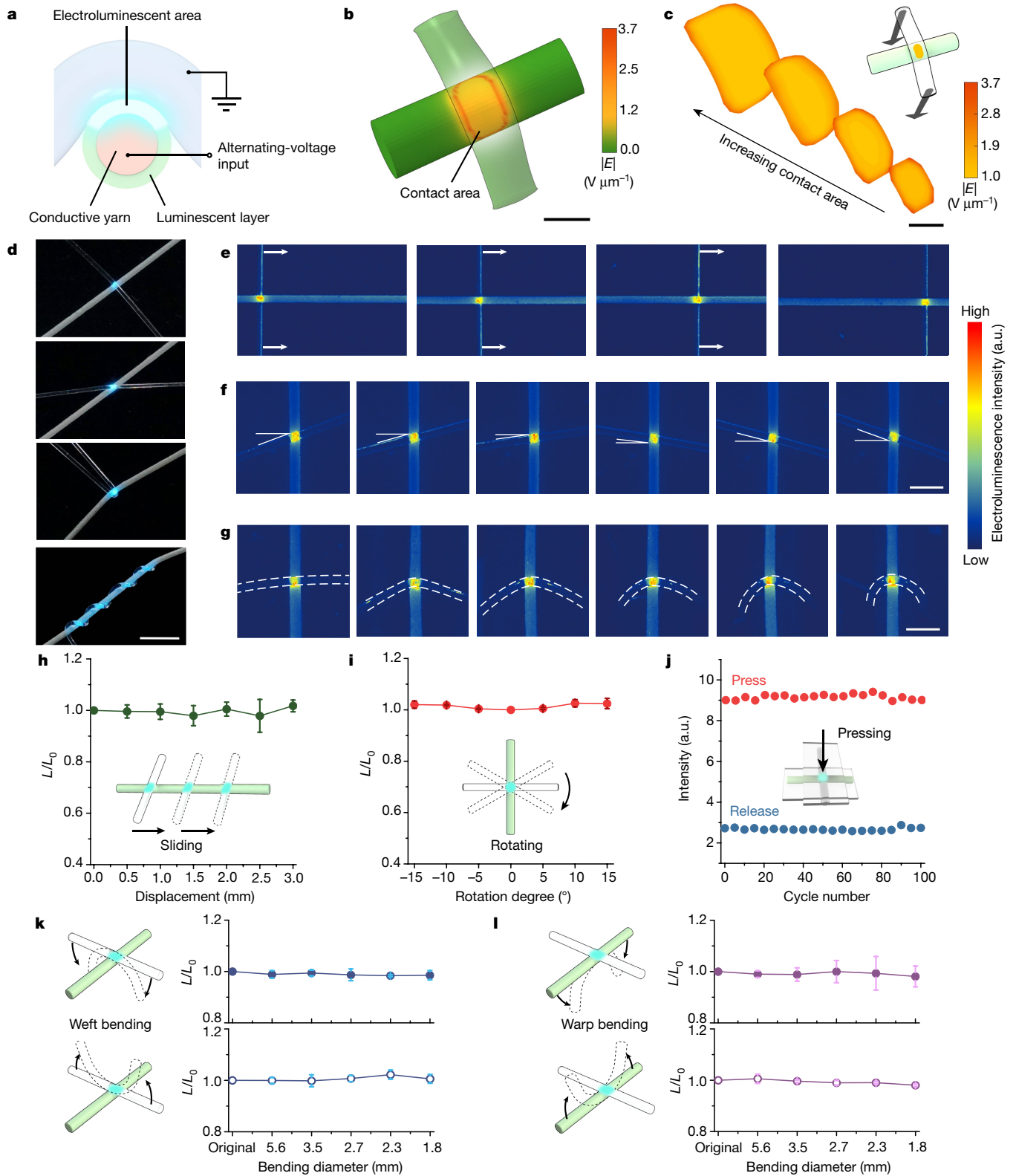


Fig. 2 | Characterization of EL units of the display textile. **a**, Schematic of an EL unit formed at the contact area between the luminescent warp and the transparent conductive weft. Light emission occurs when an alternating electric voltage is applied. **b, c**, Simulation using a finite-element method shows that the electric field distribution at the contact area in an EL unit is uniform (**b**) and does not change with increasing contact areas (**c**). **d**, Photographs show stable light emission as the transparent conductive weft is contacted, leaned, twisted and knotted with the luminescent warp (top to bottom). Scale bar, 2 mm. **e–g**, Electroluminescence maps show that the brightness of the EL units remains stable even when the transparent weft is slid

(**e**), rotated (**f**) and bent (**g**) along the luminescent warp. The colour bar indicates the relative electroluminescence intensity (see Methods section ‘Structure and performance characterization of the EL units’). Scale bars, 1 mm. **h–l**, The luminance varied minimally when the transparent weft is moved by 3 mm along the luminescent warp (**h**) and rotated by different degrees (**i**; 0° is when the weft is perpendicular to the warp), and when the EL unit is pressed and released for 100 cycles (**j**), bent along the weft length (**k**) and along the warp length (**l**) with increasing bending angles. L_0 and L correspond to the electroluminescence intensity before and after deformation, respectively. Error bars are standard deviations of the results from at least three samples.

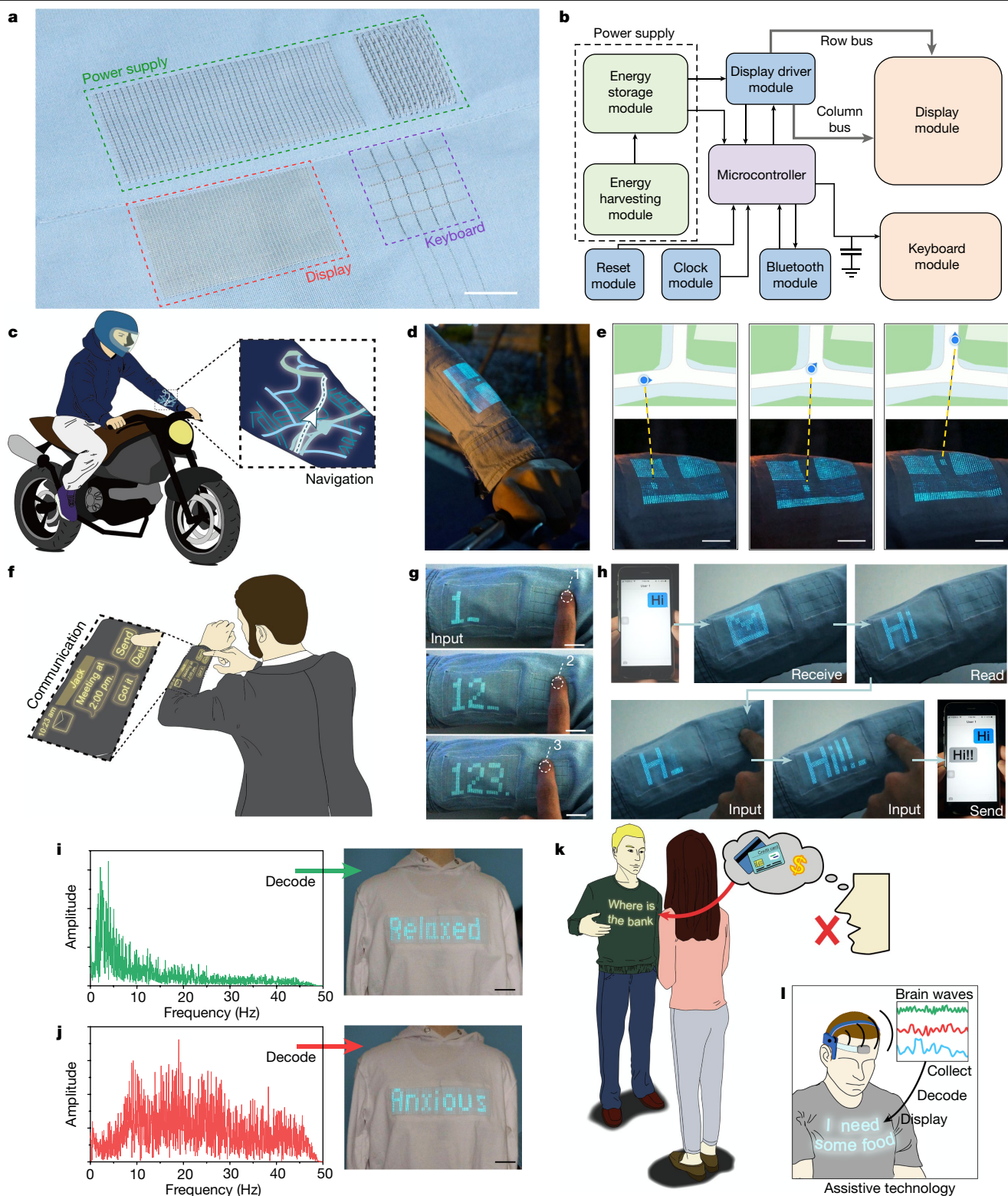


Fig. 3 | Application scenarios of integrated textile systems. **a**, Photograph of an integrated textile system consisting of display, information input (keyboard) and power supply modules. Scale bar, 2 cm. **b**, System-level block diagram of the integrated textile system in **a** shows the modules connected to a microcontroller that is powered by solar-energy harvesting and electrical energy storage modules. **c**, Conceptual image illustrating the integrated textile as a smart node for the Internet of Things to offer location services during driving. Selective illumination on the display module is achieved by scanning electrical signals from the driver circuit row by row onto the array of EL units. **d, e**, The real-time location at a T-junction is displayed on a sleeve. The information is transferred through the Bluetooth and microcontroller modules, and is synchronized with the location map on a smartphone. Scale bars, 1 cm. **f**, Conceptual image shows

that textiles integrated with a display and keyboard can be used as a communication platform. **g**, Information is input onto the clothing by pressing the keys that are woven into the textile. Scale bars, 2 cm. **h**, Receiving and sending messages between the integrated textile system and a smartphone. **i, j**, Expressions of mental states by decoding representative electroencephalogram signals. The words 'Relaxed' (**i**) and 'Anxious' (**j**) are displayed on clothes when the dominant brain waves are detected in the low-frequency region (0–10 Hz) and high-frequency region (10–40 Hz), respectively. Scale bars, 5 cm. **k**, Display textiles could in the future enable communication via clothing. **l**, Conceptual image of an assistive-technology device, showing brain waves being decoded into messages that are displayed on a shirt made from an integrated textile.

sent, received and displayed between our integrated textile system and a smartphone (Fig. 3h).

To demonstrate the potential of display textiles in healthcare, we also fabricated a large display textile measuring 24 cm × 6 cm (length × width) (Extended Data Fig. 10). We collected electroencephalogram signals from volunteers playing a race car game and those who were meditating. The brain waves in relaxed volunteers were mostly low frequency (Fig. 3i), and those in anxious volunteers were mostly high frequency³³ (Fig. 3j). We processed the signals on a computer and sent words corresponding to the mental state of the respective volunteers to the microcontroller through the Bluetooth module for display. In the future, together with ways to decode complicated brain waves, we envision display textiles such as ours to become effective assistive-technology communication tools³⁴ (Fig. 3k, l).

In summary, we present a functional, large-area display textile by weaving conductive and luminescent fibres with cotton yarn to form EL units directly within the textile. Our method is simple and can be used to weave other electronic functions such as a keyboard and power supply into the textile to form a multifunctional integrated textile system for various applications. Because of the network of wefts and warps, each EL unit in our display textile can be uniquely identified and lit in a programmable way using a driver circuit. We show that such an electronic textile can be useful as a communication tool. With the integration of more functionality, we expect these 'smart textiles' to form the communication tools of the future.

Online content

Any methods, additional references, Nature Research reporting summaries, source data, extended data, supplementary information, acknowledgements, peer review information; details of author contributions and competing interests; and statements of data and code availability are available at <https://doi.org/10.1038/s41586-021-03295-8>.

- Larson, C. et al. Highly stretchable electroluminescent skin for optical signaling and tactile sensing. *Science* **351**, 1071–1074 (2016).
- Tan, Y. J. et al. A transparent, self-healing and high- κ dielectric for low-field-emission stretchable optoelectronics. *Nat. Mater.* **19**, 182–188 (2020).
- Tian, X. et al. Wireless body sensor networks based on metamaterial textiles. *Nat. Electron.* **2**, 243–251 (2019).
- Chen, G. R., Li, Y. Z., Bick, M. & Chen, J. Smart textiles for electricity generation. *Chem. Rev.* **120**, 3668–3720 (2020).
- Weng, W., Chen, P. N., He, S. S., Sun, X. M. & Peng, H. S. Smart electronic textiles. *Angew. Chem. Int. Ed.* **55**, 6140–6169 (2016).
- Carey, T. et al. Fully inkjet-printed two-dimensional material field-effect heterojunctions for wearable and textile electronics. *Nat. Commun.* **8**, 1202 (2017).
- Kim, J. et al. Ultrathin quantum dot display integrated with wearable electronics. *Adv. Mater.* **29**, 1700217 (2017).
- Son, D. et al. An integrated self-healable electronic skin system fabricated via dynamic reconstruction of a nanostructured conducting network. *Nat. Nanotechnol.* **13**, 1057–1065 (2018).
- Yin, D. et al. Efficient and mechanically robust stretchable organic light-emitting devices by a laser-programmable buckling process. *Nat. Commun.* **7**, 11573 (2016).
- Rein, M. et al. Diode fibres for fabric-based optical communications. *Nature* **560**, 214–218 (2018).
- Leber, A. et al. Soft and stretchable liquid metal transmission lines as distributed probes of multimodal deformations. *Nat. Electron.* **3**, 316–326 (2020).
- Yang, A. N. et al. Fabric organic electrochemical transistors for biosensors. *Adv. Mater.* **30**, 1800051 (2018).
- Hatamvand, M. et al. Recent advances in fiber-shaped and planar-shaped textile solar cells. *Nano Energy* **71**, 104609 (2020).
- Jinno, H. et al. Stretchable and waterproof elastomer-coated organic photovoltaics for washable electronic textile applications. *Nat. Energy* **2**, 780–785 (2017).
- Koo, J. H., Kim, D. C., Shim, H. J., Kim, T. H. & Kim, D. H. Flexible and stretchable smart display: materials, fabrication, device design, and system integration. *Adv. Funct. Mater.* **28**, 1801834 (2018).
- de Mulatier, S., Nasreldin, M., Delattre, R., Ramuz, M. & Djenizian, T. Electronic circuits integration in textiles for data processing in wearable technologies. *Adv. Mater. Technol.* **3**, 1700320 (2018).
- Wang, B. H. & Facchetti, A. Mechanically flexible conductors for stretchable and wearable e-skin and e-textile devices. *Adv. Mater.* **31**, 1901408 (2019).
- Prieto-Ruiz, J. P. et al. Enhancing light emission in interface engineered spin-OLEDs through spin-polarized injection at high voltages. *Adv. Mater.* **31**, 1806817 (2019).
- Choi, S. et al. Highly flexible and efficient fabric-based organic light-emitting devices for clothing-shaped wearable displays. *Sci. Rep.* **7**, 6424 (2019).
- Fukagawa, H. et al. Long-lived flexible displays employing efficient and stable inverted organic light-emitting diodes. *Adv. Mater.* **30**, 1706768 (2018).
- Conaghan, P. J. et al. Highly efficient blue organic light-emitting diodes based on carbene-metal-amides. *Nat. Commun.* **11**, 1758 (2020).
- Koncar, V. Optical fiber fabric displays. *Opt. Photonics News* **16**, 40–44 (2005).
- Zhang, Z. T. et al. A colour-tunable, weavable fibre-shaped polymer light-emitting electrochemical cell. *Nat. Photon.* **9**, 233–238 (2015).
- Dias, T. & Monaragala, R. Development and analysis of novel electroluminescent yarns and fabrics for localized automotive interior illumination. *Text. Res. J.* **82**, 1164–1176 (2012).
- Liang, G. J. et al. Coaxial-structured weavable and wearable electroluminescent fibers. *Adv. Electron. Mater.* **3**, 1700401 (2017).
- Hu, D., Xu, X., Miao, J. S., Gidron, O. & Meng, H. A stretchable alternating current electroluminescent fiber. *Materials* **11**, 184 (2018).
- Zhou, Y. et al. Bright stretchable electroluminescent devices based on silver nanowire electrodes and high- κ thermoplastic elastomers. *ACS Appl. Mater. Interfaces* **10**, 44760–44767 (2018).
- Li, S., Peele, B. N., Larson, C. M., Zhao, H. C. & Shepherd, R. F. A stretchable multicolor display and touch interface using photopatterning and transfer printing. *Adv. Mater.* **28**, 9770–9775 (2016).
- Zhang, Z. T. et al. A stretchable and sensitive light-emitting fabric. *J. Mater. Chem. C* **5**, 4139–4144 (2017).
- Yang, C. H., Chen, B. H., Zhou, J. X., Chen, Y. M. & Suo, Z. G. Electroluminescence of giant stretchability. *Adv. Mater.* **28**, 4480–4484 (2016).
- Chen, F. & Xiang, Y. in *Luminescent Materials and Applications* (ed. Kitai, A.) Ch. 8 (John Wiley & Sons, 2008).
- Jin, M. L. et al. An ultrastable ionic chemiresistor skin with an intrinsically stretchable polymer electrolyte. *Adv. Mater.* **30**, 1706851 (2018).
- Müller-Putz, G. R., Riedl, R. & Wriessnegger, S. C. Electroencephalography (EEG) as a research tool in the information systems discipline: foundations, measurement, and applications. *Comm. Assoc. Inform. Syst.* **37**, 912–948 (2015).
- Voice, speech and language research <https://www.nidcd.nih.gov/about/strategic-plan/2017-2021-nidcd-strategic-plan#sp22> (National Institute on Deafness and Other Communication Disorders, accessed 8 August 2020).

Publisher's note Springer Nature remains neutral with regard to jurisdictional claims in published maps and institutional affiliations.

© The Author(s), under exclusive licence to Springer Nature Limited 2021

Preparation of the transparent conductive weft

Polyurethane ionic gel fibre was spun from the transparent ionic-liquid-doped polyurethane gel. Thermoplastic polyurethane (TPU) (Desmopan 2786A, Covestro) was first dissolved in N,N-dimethylformamide (DMF) (Sinopharm) with a weight ratio of 1/4 under mechanically stirring at 80 °C for 2 h. Subsequently, 1-ethyl-3-methylimidazolium:bis(trifluoromethylsulfonyl) imide ([EMIM]⁺[TFSI]⁻) ionic liquid (Aladdin) was added to the above TPU–DMF solution for further stirring (80 °C for 1 h). The ionic gel flake was obtained by totally removing the solvent of DMF in an oven box at 80 °C for 12 h. Then, melt-spinning was carried out using a 3D printing system (3D Bio-Architect work station, Regenovo) with a 0.25-mm inner-diameter nozzle. The transparent conductive weft was extruded at a melting zone temperature of 180 °C and cooled at room temperature. To achieve water resistance, a silicone protective layer (I-2577, Dow Corning) was further dip-coated on the transparent conductive wefts.

Preparation of the luminescent warp

Commercially available ZnS phosphors (Shanghai Keyan Phosphor Technology Co.) were dispersed in waterborne polyurethane (U-9, Shanghai Sisheng Polymer Materials Co.) with a weight ratio of 3/1 by mechanical stirring for 20 min. After degassing in a vacuum oven, the as-prepared mixtures were loaded on the silver-plated nylon yarns (100D, Hengtong X-silver Speciality Textile Co.) on a continuous producing line. Silver-plated yarns were dipped into the ZnS phosphor dispersions and passed through the centre of a scraper ring in inner diameter of 0.32 mm, followed by drying under 120 °C in a 2-m-long air-dry oven. The movement speed of the yarns was 10 m min⁻¹. A coating process was conducted three times to prepare the luminescent warp in a diameter of approximately 0.3 mm. To achieve water resistance, a silicone protective layer (I-2577, Dow Corning) was further dip-coated on the luminescent warps.

Fabrication of the display textile

The weaving operation of the display textile was made on a rapier loom (Tong Yuan Textile Machinery Co.). The weave diagram is presented in Fig. 1a. Note that other fibre materials such as polyurethane-coated metal wire can be also co-woven inside.

Structure and performance characterization of the EL units

The cross-sectional image in Extended Data Fig. 1i of the single EL unit was obtained from scanning electron microscopy (S-4800, Hitachi) operated at 1 kV. The photographs of the textile were captured by a digital camera (D3400, Nikon) unless specified. The transparency of the ionic gel was characterized by an ultraviolet–visible spectrophotometer (UV-2550 Spectrometer, Shimadzu) to scan wavelengths from 450 to 700 nm. The luminance of a single EL unit was detected by a spectrophotometer (PhotoResearch PR-680) under an alternating voltage supplied by a function waveform generator (Keysight 33500B Series) connected with a high-voltage power amplifier (610 E, TREK). If not specified, the test parameters of the EL unit were 1.2 V μm⁻¹ and 2 kHz, and the intersection area in the EL unit projection was used as the effective device area. The voltage, current and power consumption were measured (34461A digital multimeter, Keysight) using a test circuit (see Extended Data Fig. 4e for details). The electroluminescence mappings of EL units under bending, sliding and rotating were obtained by mapping the photographs in Matlab. The relative electroluminescence intensity was defined according to the grey value. For the statistical analysis of the relative electroluminescence intensity of the units in the display textile (Fig. 1c–g, Extended Data Fig. 3), the grey values of the units were extracted from the photographs by ImageJ. The photographs were captured by a scientific camera (Photometrics Prime BSI) in a dark room. The calibration curve of grey

values against actual luminance (detected by the photodetector) was made before statistical analysis (Extended Data Fig. 4f). The grey values were linearly correlated with the luminance of the unit, indicating that the statistical analysis of the emission variations based on the grey values was reliable. The uniformity of the EL unit array was evaluated according to the relative deviation, calculated by $RD = ((L_x - \bar{L})/\bar{L}) \times 100\%$, where L_x was the electroluminescence intensity of a single EL unit, and \bar{L} was the average intensity of 600 units. The stability of the EL unit array was evaluated by counting the electroluminescence intensity variation (calculated as L/L_0 , where L_0 and L were the intensities before and after deforming, respectively) of 600 EL units. The temperature changes of the EL units were measured by an infrared camera (PI 640, Optris).

Washing test of the display textile

Accelerated washing tests (approximately equal to five typical home laundings) were performed in a standard washing machine (SW-12E, Nantong Hongda Experimental Instrument Co.) (Extended Data Fig. 6e) following the ISO 105/C10:2006 and AATCC 61-2013 international standards for fabric washing. The load information includes: a 4 cm × 10 cm section of the display fabric, 200 g of water, and 0.5 wt% liquid detergent. We used a washing temperature of 60 °C, and the duration for each wash was 30 min (Extended Data Fig. 6f). The stirring speed was 1,000 rpm. To evaluate the mechanical effects of washing, a total of 10 steel balls (6 mm in diameter) were added into the washing containers. After the washing test, the textiles were rinsed under flowing water and dried at 60 °C for 1 h. The test parameters of the electroluminescence performance were 3 V μm⁻¹ and 2 kHz.

Calculation of the power consumption of an EL unit

The voltage at certain positions (the root mean square at A, B, C and Ground; refer to Extended Data Fig. 4e) and the resistance of each resistor were first measured. The current across each resistor was calculated as $I = V/R$. The current through resistors 2 and 3 was:

$$I_2 = \frac{V_{AB}}{R_2} = I_3 \quad (1)$$

Using equation (1), V_{AC} was calculated (the voltage across the entire test circuit):

$$V_{AC} = V_{AB} + V_{BC} = I_2 R_2 + I_3 R_3 \quad (2)$$

The current across resistor 1 was equal to the total current through the test circuit. On the basis of this equality, the power of the test circuit was:

$$P_{\text{total}} = I_1 V_{AC} \cos \theta \quad (3)$$

where θ represents the phase shift between the current and voltage waveforms across the test circuit. This phase shift was measured using an oscilloscope (TDS 2012C, Tektronix). Hence, the real power of the test circuit—which included energy used by the EL unit and the resistors—could be calculated according to:

$$P_{\text{total}} = P_{\text{unit}} + P_{\text{resistor}} \quad (4)$$

The power consumption of the EL unit was obtained by subtracting the power consumption of the resistor. The power consumed by each resistor was calculated by $P = I^2 R$.

Electric field simulation of the EL unit using finite-element method

The EL unit was constructed in ABAQUS CAE with geometric characteristics given in Extended Data Fig. 1i. Eight-node linear reduced-integration hybrid brick elements (C3D8RH) were used to model the transparent

conductive weft of hyperelastic materials. Through a mesh convergence study, 30,284 and 39,840 elements were generated for the luminescent warp and the transparent conductive weft, respectively.

Mechanical properties of the materials were defined by directly importing the uniaxial tensile test data (Extended Data Fig. 1). A linear elastic model was used for the luminescent warp. An Ogden hyperelastic model was used for the polyurethane ionic gel fibre with the strain energy potential function W :

$$W = \frac{2\mu_1}{\alpha_1^2} (\bar{\lambda}_1^{\alpha_1} + \bar{\lambda}_2^{\alpha_1} + \bar{\lambda}_3^{\alpha_1} - 3) + \frac{1}{D_1} (J - 1)^2,$$

where $\bar{\lambda}_i$ is the deviatoric principal stretches, $\bar{\lambda}_i = J^{-1/3} \lambda_i$ and λ_i is the principal stretches. This form can be degenerated into neo-Hookean form of potential energy when $\alpha_1 = 2$.

As mentioned above, periodic boundary conditions were imposed along the axial direction of the transparent conductive weft. The axial length of an EL unit was fixed, because the weft was kept tight during the weaving process. Contact between the transparent conductive weft and the luminescent warp was defined as default hard contact. The loads imposed on both ends of the transparent conductive weft were estimated by outputting the reaction force of the polyurethane ionic gel fibre under a displacement of 0.48 mm.

Static electric analyses were then conducted on the deformed models to obtain the electric fields in the ZnS phosphor layer. The transparent conductive weft was grounded and 90 V electric potential was imposed on the core conductive yarn of luminescent warp. The dielectric constant of the luminescent layer was $3.621 \times 10^{-11} \text{ F m}^{-1}$.

Fabrication of the textile keyboard

The textile keyboard was based on a jacquard method by weaving carbon fibres (1K, TORAY), silver-plated yarns and cotton yarns according to the weave diagram in Extended Data Fig. 7a. Pressing a key activates it, and releasing turns it off (Extended Data Fig. 7d, e). The keyboard works by reading the voltage between the metallic and carbon fibres (sample voltage, V_s) under an applied voltage (V_{cc}) of 5 V. Each key in the 4×4 keyboard is distinguished by the different sample voltage recorded when the key is pressed (Extended Data Fig. 7f).

Fabrication of the energy harvesting and storing textile

Ti wire (diameter of 127 μm , Alfa Aesar) was used as the substrate of the photoanode. First, the Ti wire was sequentially cleaned by sonication in deionized water, acetone and isopropanol for 5 min each. Then TiO₂ nanotubes were grown on the Ti wire by an anodic oxidation in a water bath. A 0.3 wt% NH₄F/ethylene glycol (Sinopharm) solution containing 8 wt% H₂O was prepared as the electrolyte. The growth was operated in a two-electrode system with the Ti wire as the anode and a Pt plate as the cathode at 60 V for 2 h. The modified Ti wire was washed and annealed at 500 °C for 60 min. After cooled to 110 °C in the furnace, the wire was immersed in Z907 (Shanghai MaterWin New Materials Co.) solution (a 0.3 mM solvent mixture of dehydrated acetonitrile (Adamas) and tert-butanol (Sinopharm) with an equal volume ratio) for 16 h. Next, CuI was drop-coated onto the modified Ti wire in a glovebox at 110 °C. A CuI solution was prepared by dissolving 0.16 M cuprous iodide (Aladdin), 1-methyl-3-ethylimidazolium thiocyanate (Lanzhou Greenchem ILs) and 0.2 mM 4-tert-butylpyridine (Adamas) in acetonitrile. Owing to the close contact between the photoanode wefts and the conductive yarns, the electric outputs of the photovoltaic textile remained stable when it was bent from 0° to 180° (Extended Data Fig. 8g). Even after 10,000 cycles of bending, the electric output and structure of the photoanode fibre were well maintained (Extended Data Fig. 8h, i). The bending radius was 4 mm.

The aqueous zinc-ion battery fibre was composed of a MnO₂ coated carbon nanotube fibre cathode, a zinc wire anode, and gelatin/ZnSO₄

water-based gel electrolyte³⁵. A carbon nanotube fibre was first synthesized by the floating-catalyst method³⁶. For the fibre cathode, MnO₂ was electrodeposited onto the carbon nanotube fibre through a scalable electrodeposition method (pulse mode 1.5 V for 1 s and 0.7 V for 10 s) in electrolyte containing 0.1 M Mn(Ac)₂·4H₂O (Aladdin) and 0.1 M Na₂SO₄ (Sinopharm) with an Ag/AgCl reference electrode and a Pt counter electrode. The MnO₂ loading mass was 0.5 mg cm⁻¹ for the cathode fibre. The zinc wire, with a diameter of ~0.5 mm, was polished and rinsed before use. The cathode and anode wires were uniformly coated with gel electrolyte and then twisted together. The gel electrolyte was prepared by first dissolving 1.0 g gelatin (Sinopharm) and 0.1 g Na₂B₄O₇ (Aladdin) in 10 ml deionized water at 80 °C. Then 10 mM ZnSO₄·7H₂O (Aladdin) and 1 mM MnSO₄·H₂O (Aladdin) were added under stirring until a homogenous solution was formed. The as-fabricated battery was dried at room temperature. The gel electrolyte acted as both an electrolyte and separator. The battery, composed of the twisted cathode and anode wires, was put into a flexible poly(vinyl chloride) (PVC) tube (ranging from hundreds of micrometres to several millimetres in diameter) and sealed by resin adhesive at the terminals of the tube. The PVC-encapsulated battery fibre withstood bending and retained a capacity of >80% after 10,000 cycles of bending (Extended Data Fig. 8m, n). The bending radius was 4 mm.

Silver-plated nylon yarns were woven in the warp direction as the counter electrodes for the energy harvesting part and the electrical connections for the energy storage part. The cotton threads, modified photoanode fibres and zinc-ion battery fibres were then alternately woven in the weft direction. Current density–voltage curves of the energy harvesting part were recorded by a Keithley 2400 source meter under the illumination (100 mW cm⁻²) of simulated AM1.5 solar light from a solar simulator (Oriel-Sol3A 94023A, equipped with a 450 W Xe lamp and an AM1.5 filter). The area marked by the dashed line in Extended Data Fig. 8a was used to calculate the current density. Electrochemical measurements were performed on an electrochemical workstation (CHI 660a).

Fabrication of the integrated textile system

Different electronic textiles were arranged on a piece of cloth by changing functional fibres during the weaving process, which were integrated on a jacket by hot-melt adhesive or sewing (Extended Data Fig. 9a–c). The microcontroller of textile electronics was STM-32F103T8U6, an ARM 32-bit Cortex TM-M3 CPU with QFN36 package (DM14580). The single-bus detection of the keyboard was realized using an analogue-to-digital converter to sample the keyboard resistance. The driving circuit of the display textile was provided by Shanghai Mi Fang Electronics Co. The communication between the integrated textile system and the mobile phone was realized using a Bluetooth module (HC-05). The power supply of the integrated textile system was provided by battery fibres that stored energy from the photovoltaic textile module. For the integration circuit, the conductive wefts and luminescent warps of the display textile were connected to the display driver module by connecting lines named as column and line buses. The display driver module and microcontroller (integrated with reset and clock modules) were connected to the energy storage module (fibre batteries). The keyboard and Bluetooth modules were connected to the microcontroller. Display driver module, microcontroller and Bluetooth module were connected to form the external controlling device system, which was inserted in a pocket on the arm sleeve (Extended Data Fig. 9b).

To connect the circuits to the textile, flexible and thin conductive fibres serving as connecting lines were sewn into the textile using a digital sewing machine (Extended Data Fig. 9c). The conductive fibres were neatly arranged in the textile according to the designed sewing circuit patterns (Extended Data Fig. 9d–g). Thereafter, the conductive fibres were carefully connected to the warp and weft electrodes of the display textile using mature welding equipment.

Article

The connecting points remained robust even when bent (Extended Data Fig. 9h, i).

Collection and decoding of electroencephalogram signals

The signals of volunteers were collected by a wearable recorder (Mind-Wave Mobile 2, Neurosky). The volunteers were asked to play a car racing game to be in an anxious mental state and lay back in meditation to be in a relaxed mental state. The signals were recorded in real time and collected on a computer. After downsampling to 100 Hz, the signals were filtered by 4th-order IIR bandpass filters with bandwidth of 0.1–48 Hz. The time-domain signals were transferred to spectrogram by fast Fourier transform.

Data availability

The data that support the findings of this study are available from figshare at https://figshare.com/articles/dataset/Source_data_Display_textile_rar/13573205. Source data are provided with this paper.

Code availability

The codes used for the integrated textile system in this study are available at https://github.com/hnsyzjianghan/textiles_display.

35. Wang, Z. F. et al. A flexible rechargeable zinc-ion wire-shaped battery with shape memory function. *J. Mater. Chem. A* **6**, 8549–8557 (2018).
36. Lee, J. et al. Direct spinning and densification method for high-performance carbon nanotube fibers. *Nat. Commun.* **10**, 2962 (2019).

Acknowledgements This work was supported by MOST (2016YFA0203302), NSFC (21634003, 22075050, 21805044), STCSM (20JC1414902, 18QA1400700, 19QA1400800) and SHMEC (2017-01-07-00-07-E00062). Part of the sample fabrication was performed at the Fudan Nano-fabrication Laboratory. We thank Shanghai Mi Fang Electronics Co., Ltd for technical support of the display driving circuits, Idea Optics Co., Ltd for offering test instruments, J. Zhao for assistance in textile weaving, and A. L. Chun of Science Storylab for critically reading and editing the manuscript.

Author contributions H.P. and P.C. conceived and designed the research project. X. Shi., Y.Z. and P.Z. performed the experiments on the display textile, keyboard and integration systems. J.S., Y.Y. and Q.T. performed the simulation. Z.G. performed the experiments on photovoltaic textiles. M.L. and J. Wang performed the experiments on energy storage fibres. J. Wu and B.W. performed the durability test. X. Shi, Y.Z., P.Z. and X.X. analysed the data. B.Z., X. Sun., L.Z., Q.P., D.J. and all other authors discussed the data and wrote the paper.

Competing interests The authors declare no competing interests.

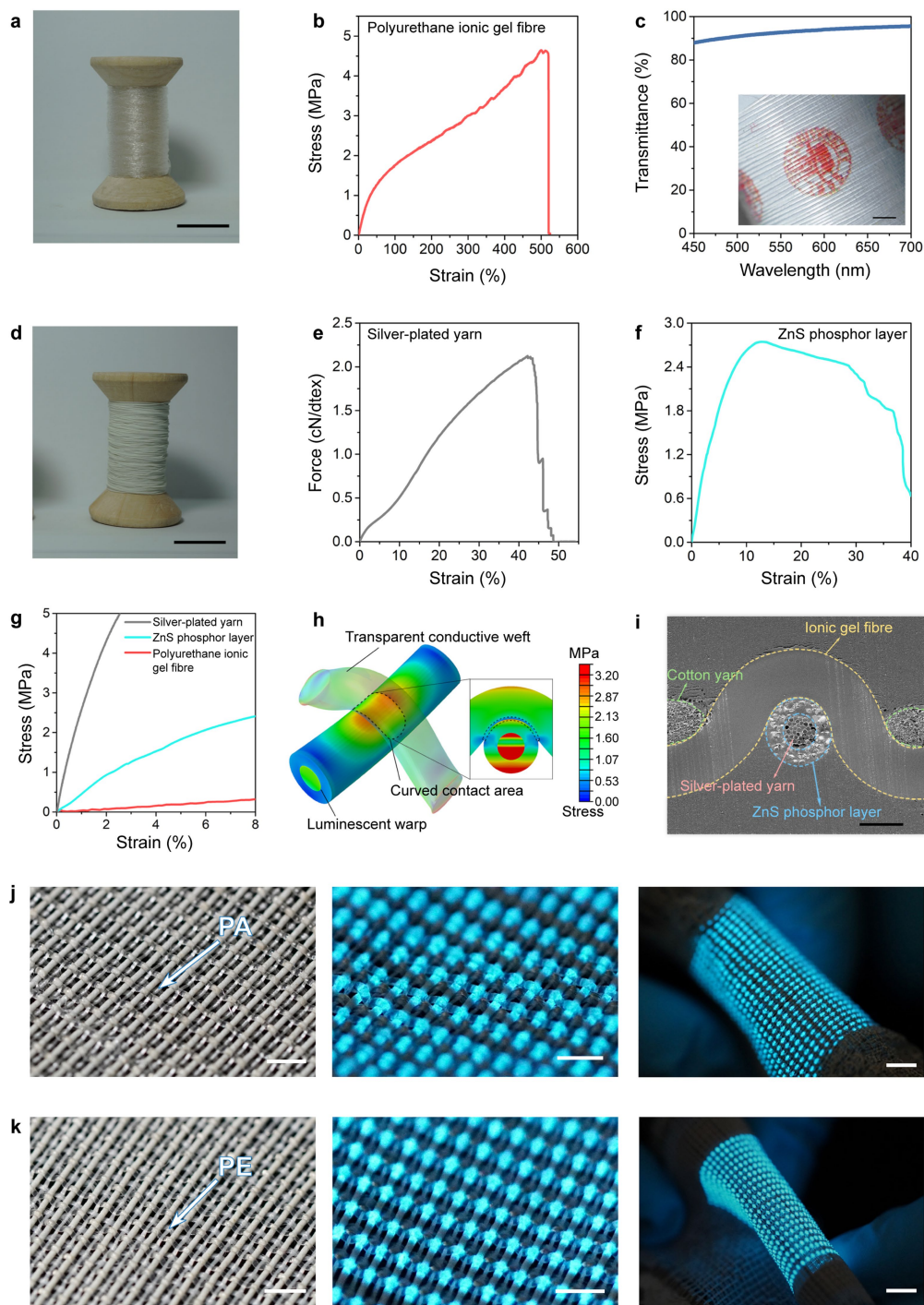
Additional information

Supplementary information The online version contains supplementary material available at <https://doi.org/10.1038/s41586-021-03295-8>.

Correspondence and requests for materials should be addressed to P.C. or H.P.

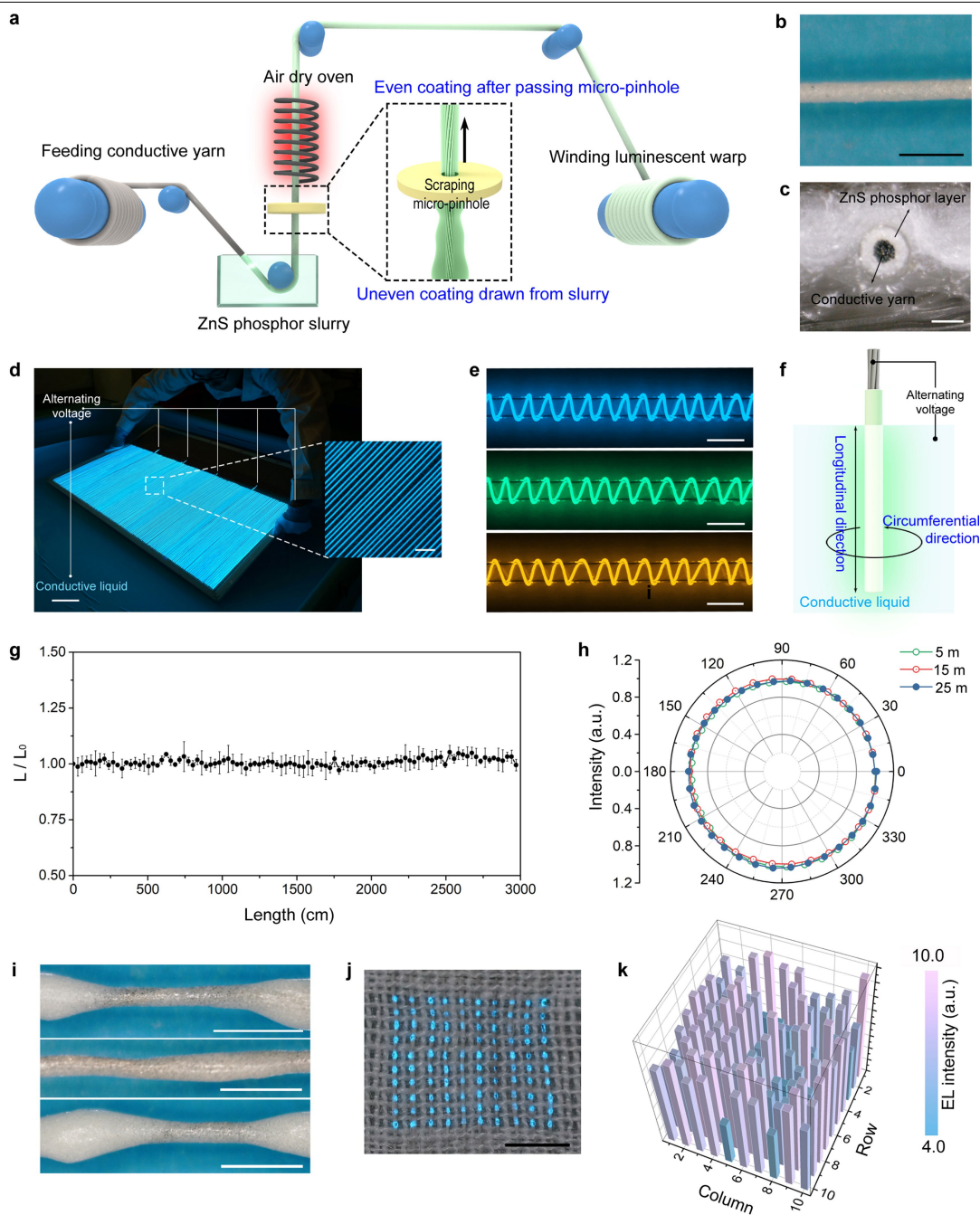
Peer review information *Nature* thanks Tilak Dias, Xiaoming Tao and the other, anonymous, reviewer(s) for their contribution to the peer review of this work.

Reprints and permissions information is available at <http://www.nature.com/reprints>.



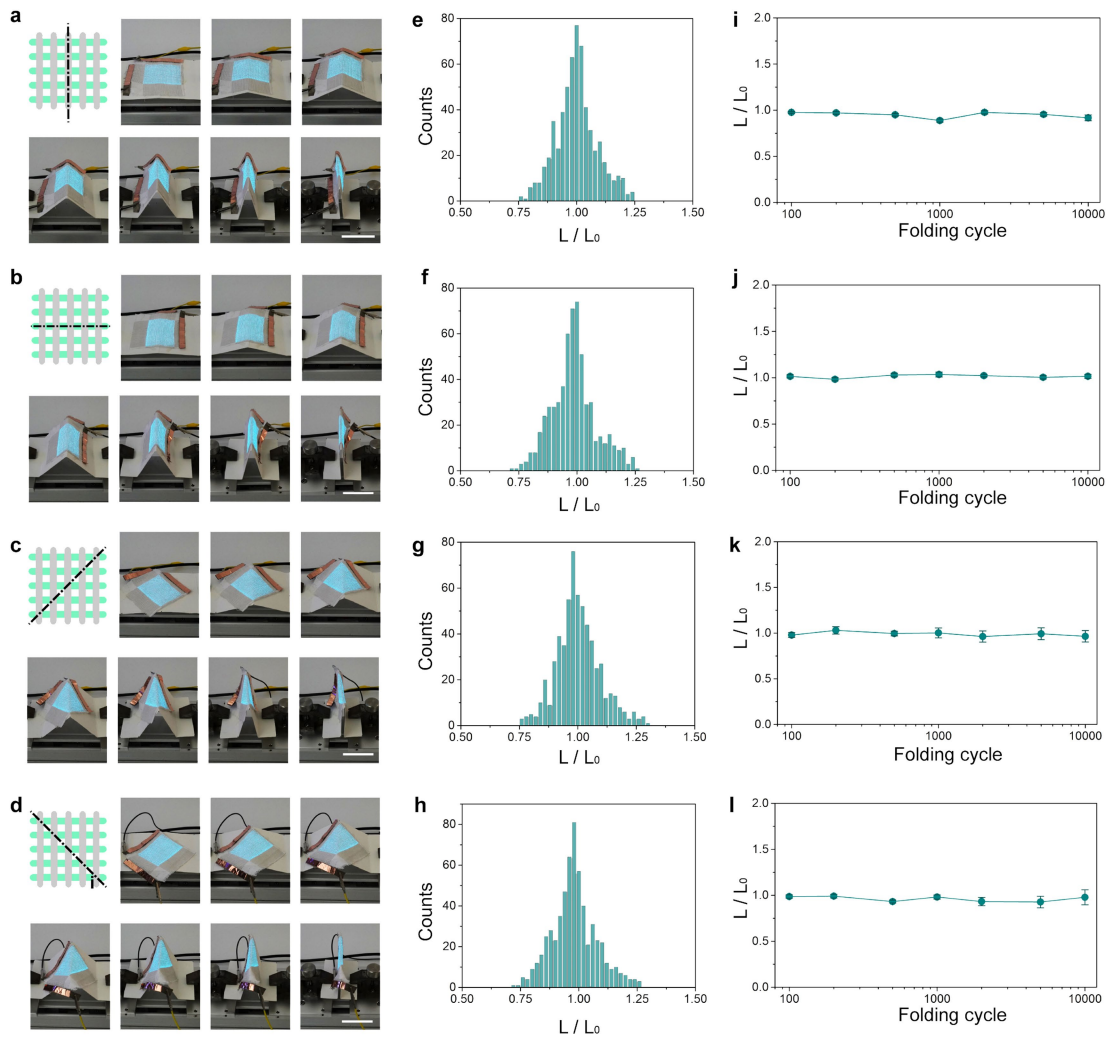
Extended Data Fig. 1 | Mechanical characterization of transparent conductive weft, luminescent warp and their contact area. **a**, A photograph of transparent conductive wefts on a spool. Scale bar, 2 cm. **b**, Stress-strain curve of polyurethane ionic gel fibre. **c**, Transmittance of ionic gel film with thickness of 250 μm . Inset, transparent conductive weft wound on a spool. Scale bar, 2 mm. **d**, Photograph of luminescent warps on a spool. Scale bar, 2 cm. **e**, Force-strain curve of silver-plated yarn. **f**, Stress-strain curve of ZnS

phosphor layer. **g**, Comparison of mechanical properties of silver-plated yarn, ZnS phosphor layer and polyurethane ionic gel fibre. **h**, Deformation and stress simulation in an EL unit. **i**, Cross-sectional scanning electron microscope image of an EL unit after embedding in resin. Scale bar, 200 μm . **j**, **k**, Photographs of display textiles co-woven with commercial nylon (PA) and polyester (PE) fibres, respectively. Scale bars, from left to right, 2 cm, 2 cm and 5 cm.



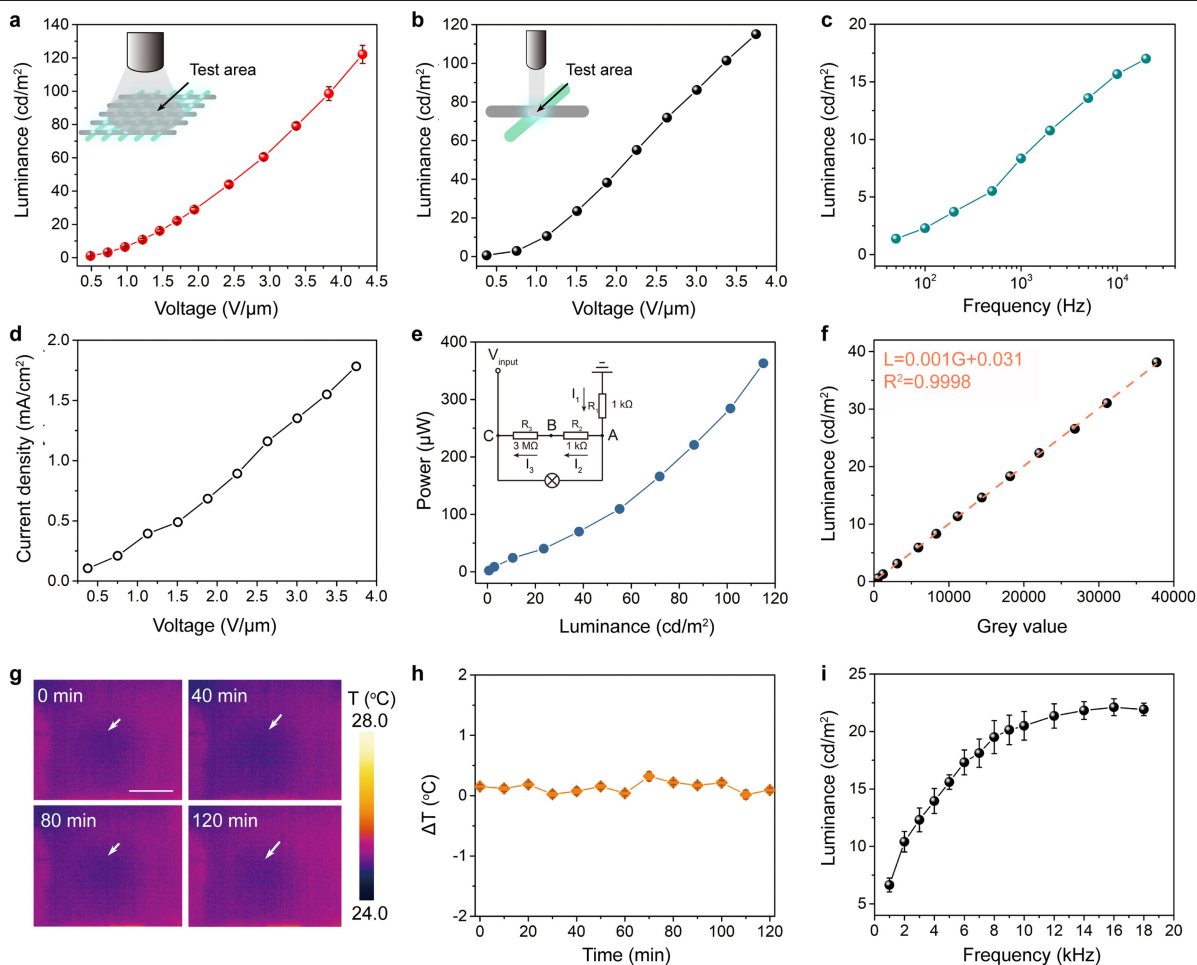
Extended Data Fig. 2 | Longitudinal and circumferential homogeneity of luminescent warp. **a**, Schematic illustration of continuous fabrication of luminescent warp. **b**, Optical image of luminescent warp. Scale bar, 1 mm. **c**, Cross-sectional image of luminescent warp. Scale bar, 200 μm . **d**, Photographs of ~100-m-long luminescent warp arranged in parallel on a board in a salt water pool. Scale bar, 10 cm. The luminescent warp was illuminated by applying an alternating voltage to the luminescent warp and salt water. The magnified area indicates the homogeneous luminescence along the fibre. Scale bar, 5 mm. **e**, Multicolour luminescent warps wound on a glass stick

and illuminated in salt water. Scale bars, 5 mm. **f**, Schematic of longitudinal and circumferential direction of luminescent warp. **g**, Luminance distribution along the length of luminescent warp. Error bars represent the standard deviations of the results from three samples. **h**, Luminance distribution around the luminescent warp circumference. **i**, Uneven luminescent layer in the case without using the scraping micro-pinhole. Scale bars, 1 mm. **j**, Photograph of the display textile woven from luminescent warps with uneven coating. Scale bar, 5 mm. **k**, Relative emission intensities of the 10×10 EL unit array in **j**.



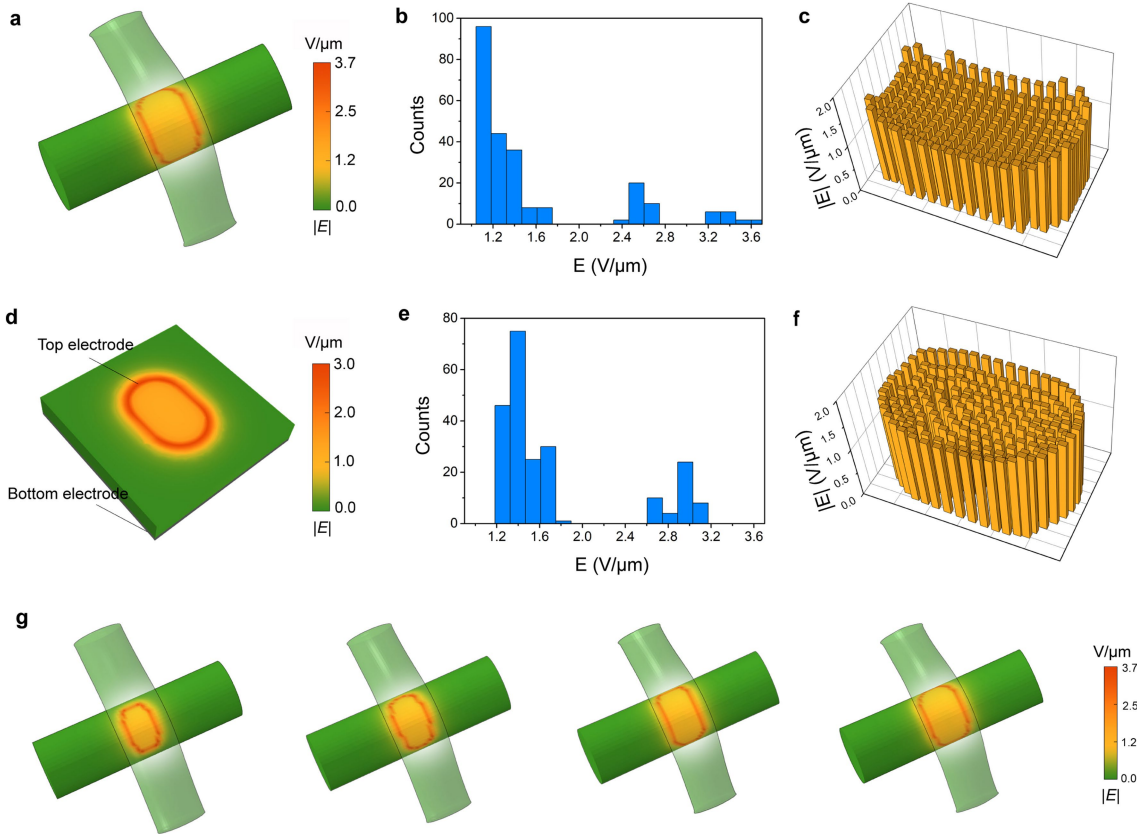
Extended Data Fig. 3 | Durability and stability of the display textile upon folding. **a–l**, Photographs (**a–d**), statistical distribution of variations in luminance of EL units of a display textile containing 600 EL units (**e–h**), and variation of the relative luminescent intensity for the EL units at the folding lines (**i–l**) when the textile was successively folded along the vertical middle line

(**a, e, i**), horizontal middle line (**b, f, j**) and diagonal lines (**c, g, k, d, h, l**) for 10,000 cycles each. The bending radius was 1 mm. The majority of the EL units showed little change. Scale bars, 5 cm. Error bars are standard deviations of the results from six samples.



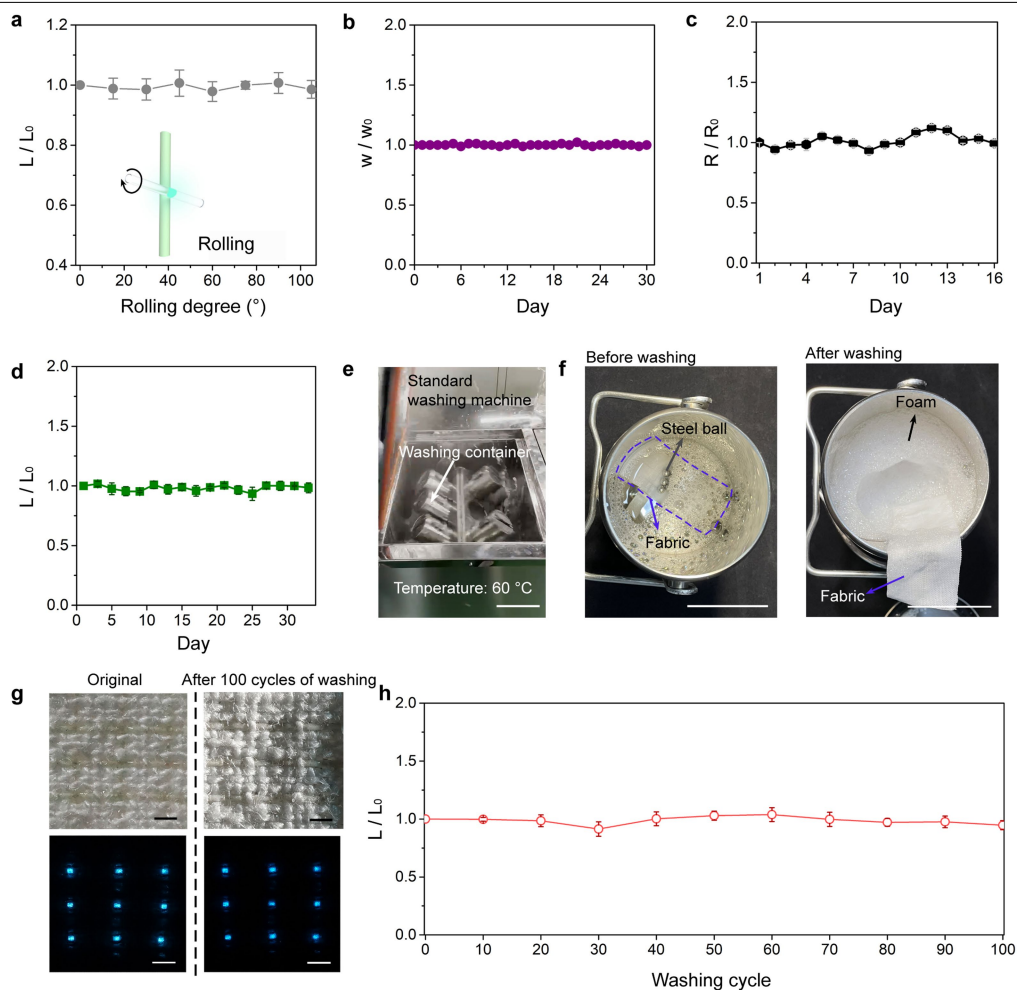
Extended Data Fig. 4 | Electroluminescence performance of the display textile and EL unit. **a**, Luminance–voltage curve of the display textile based on the projected area of the textile. **b**, **c**, Higher applied voltage (**b**) and frequency (**c**) increase the luminance of the EL unit. Frequency used in **b** was 2,000 Hz. Voltage applied in **c** was $1.2 \text{ V } \mu\text{m}^{-1}$. **d**, **e**, Current density–voltage (**d**) and power–luminance (**e**) characteristics of the EL unit. The inset of **e** shows the test circuit for measuring the power consumption of the EL unit. **f**, Calibration curve showing that the grey values extracted from photographs obtained from a

camera are linearly correlated with the actual luminance of the EL unit as detected by a photodetector. **g**, Thermal images of an EL unit illuminated for increasing durations (under a power of $\sim 300 \text{ } \mu\text{W}$). The arrows indicate the position of the EL unit. Scale bar, 5 mm. **h**, Local temperature variations of EL units under a power of $\sim 300 \text{ } \mu\text{W}$. **i**, Luminance–frequency curve of the EL unit working at 35 V. Thickness of the luminescent layer is $\sim 30 \text{ } \mu\text{m}$. Error bars represent the standard deviations of the results from at least three samples.



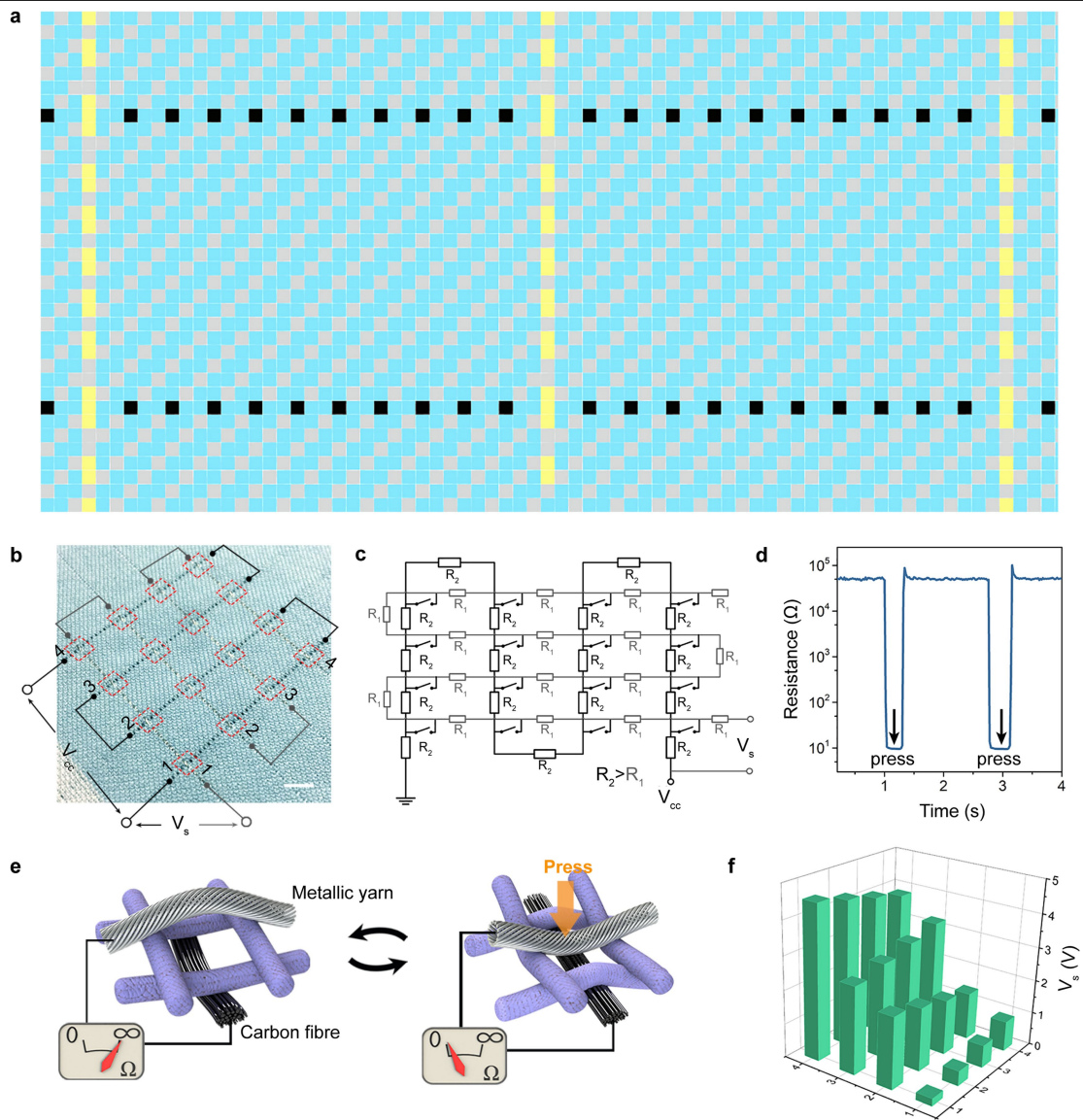
Extended Data Fig. 5 | Comparison of electric field distribution of curved and planar contact areas. Electric field distribution in woven EL unit (a–c) and traditional planar sandwiched electroluminescent devices (d–f). **a, d**, Electric field distribution. **b, e**, Statistics of the simulation elements on contact area

according to the electric field values. **c, f**, Visualization of the electric field values by the height of bars. **g**, Electric field distributions of EL unit along with increasing contact areas.



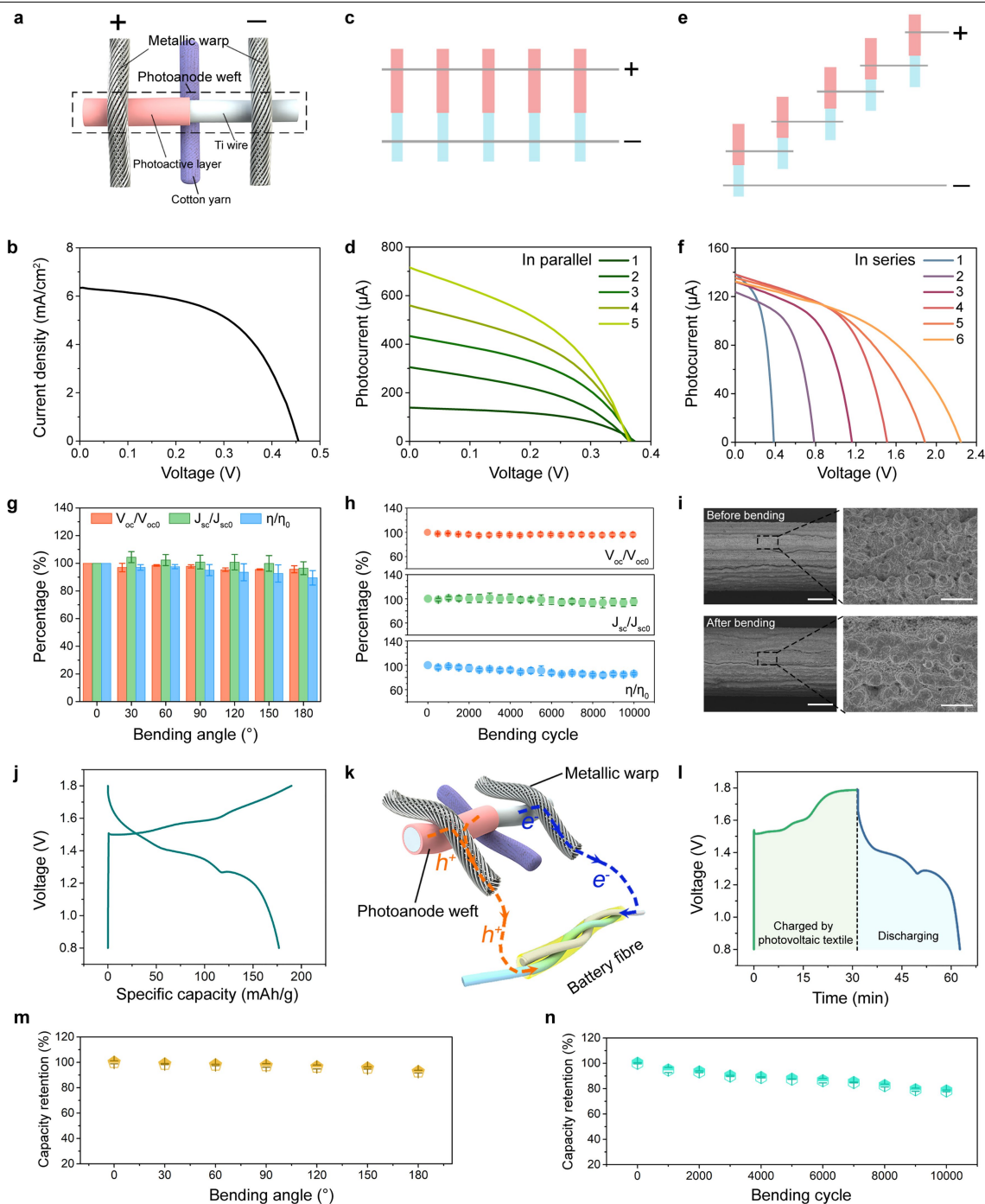
Extended Data Fig. 6 | Durability of polyurethane ionic gel fibre and EL units. **a**, Luminance variations when the transparent conductive weft is rolled around its central axis. L_0 and L correspond to the electroluminescence intensity before and after deformation, respectively. **b**, **c** Variation of weight (**b**) and electrical resistance (**c**) for the polyurethane ionic gel fibre in open air at room temperature ($-25\text{ }^\circ\text{C}$). Here w_0 and w correspond to the weights before and after exposure to the air, respectively, and R_0 and R correspond to the electrical resistances before and after exposure to the air, respectively. **d**, Electroluminescence performance of EL units stored in open air. L_0 and L correspond to the electroluminescence intensity before and after exposure to

the air, respectively. **e**, Photograph of the standard washing machine used in the washing test. Scale bar, 20 cm. **f**, Photographs of the washing container before and after washing. Scale bars, 5 cm. **g**, Photographs (top) and emission images (bottom) show that the luminescence of EL units after 100 cycles of washing (30 min per cycle) is similar to the original unwashed fabric. Scale bars, 1 mm. **h**, Quantitative measurement of the luminance of EL units. Little change is seen over 100 cycles of washing and drying. L_0 and L correspond to the electroluminescence intensities before and after washing, respectively. Error bars are standard deviations of the results from at least three samples.



Extended Data Fig. 7 | Characterization of the textile keyboard. **a**, Weave diagram of the textile keyboard (yellow: Ag-plated fibre, black: carbon fibre, blue: cotton yarn, grey: cotton yarn). **b**, Photograph and electrical connection of a 4×4 textile keyboard. The red squares indicate the positions of keys. Scale bar, 5 mm. **c**, Equivalent circuit of a 4×4 keyboard. This keyboard worked by reading the voltage between the metallic and carbon fibres (sample voltage, V_s)

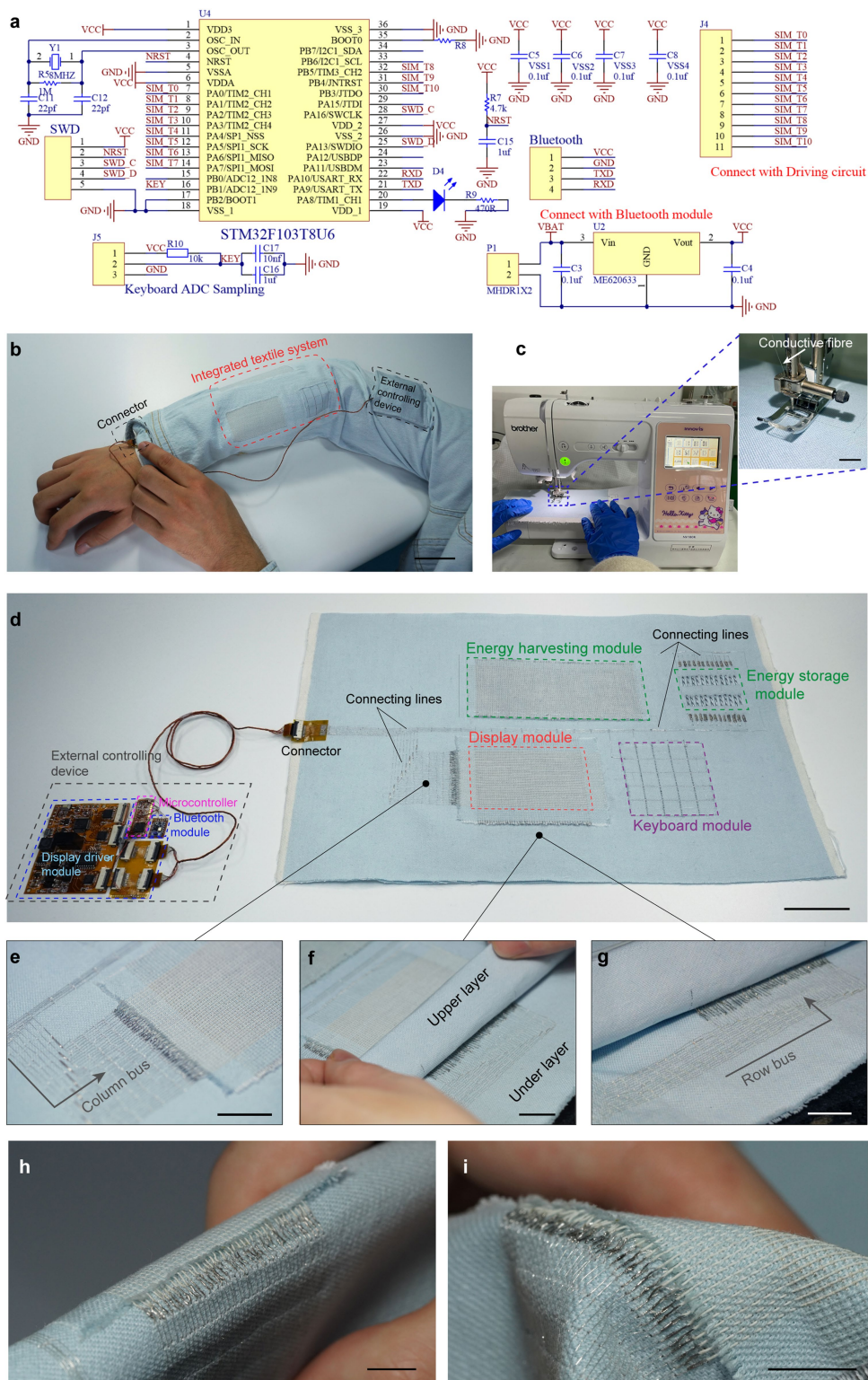
at an applied voltage (V_{cc}) of 5 V. **d**, Pressing responses of a key with resistance variations that were greater than four orders of magnitude. **e**, Working mechanism of the textile keyboard. **f**, Voltages (V_s) recorded by pressing individual keys one by one. The correspondence between the key position and its characteristic V_s are indicated by the coordinates in **b** and **f**.



Extended Data Fig. 8 | Characterization of the textile power supply system.

a, Schematic of a woven photovoltaic unit. **b**, Current density–voltage characteristics of the photovoltaic unit, exhibiting a short-circuit current density of 6.32 mA cm^{-2} and an open-circuit voltage of 0.45 V . **c**, Schematic of the woven photovoltaic units connected in parallel. **d**, Current–voltage curve of the photovoltaic textile with increasing numbers of photoanode wefts connected in parallel. **e**, Schematic of the woven photovoltaic units connected in series. **f**, Current–voltage curve of the photovoltaic textile with increasing numbers of photoanode wefts connected in series. **g**, **h**, Photovoltaic performances at different bending angles (**g**) and bending cycles at bending angle of 45° (**h**) show $<10\%$ variation. V_{oc0} and V_{oc} represent the open-circuit voltage before and after bending, respectively; J_{sc0} and J_{sc} correspond to the photocurrent density before and after bending, respectively; and η_0 and η

represent the photon-to-electron conversion efficiency before and after bending, respectively. **i**, Scanning electron microscope images of the photoanode fibre before and after 10,000 cycles of bending appear similar. Scale bars, from left to right, $50 \mu\text{m}$ and $5 \mu\text{m}$. **j**, Galvanostatic charge/discharge curves at 200 mA g^{-1} (based on the active material of the cathode). The battery fibre exhibited a mass capacity of $176.9 \text{ mA h g}^{-1}$. **k**, Schematic of the working mechanism of the energy harvesting and storage module. **l**, Photocharge and discharge curves of the battery fibre. Six photovoltaic units in series under illumination are used to charge zinc-ion battery fibres. The battery fibres are discharged to an external circuit at a current of $80 \mu\text{A}$. **m**, **n**, Capacity retention of the battery fibre after bending at different angles (**m**) and over 10,000 cycles of bending at a fixed bending angle of 45° (**n**). Error bars are standard deviations of the results from three samples.



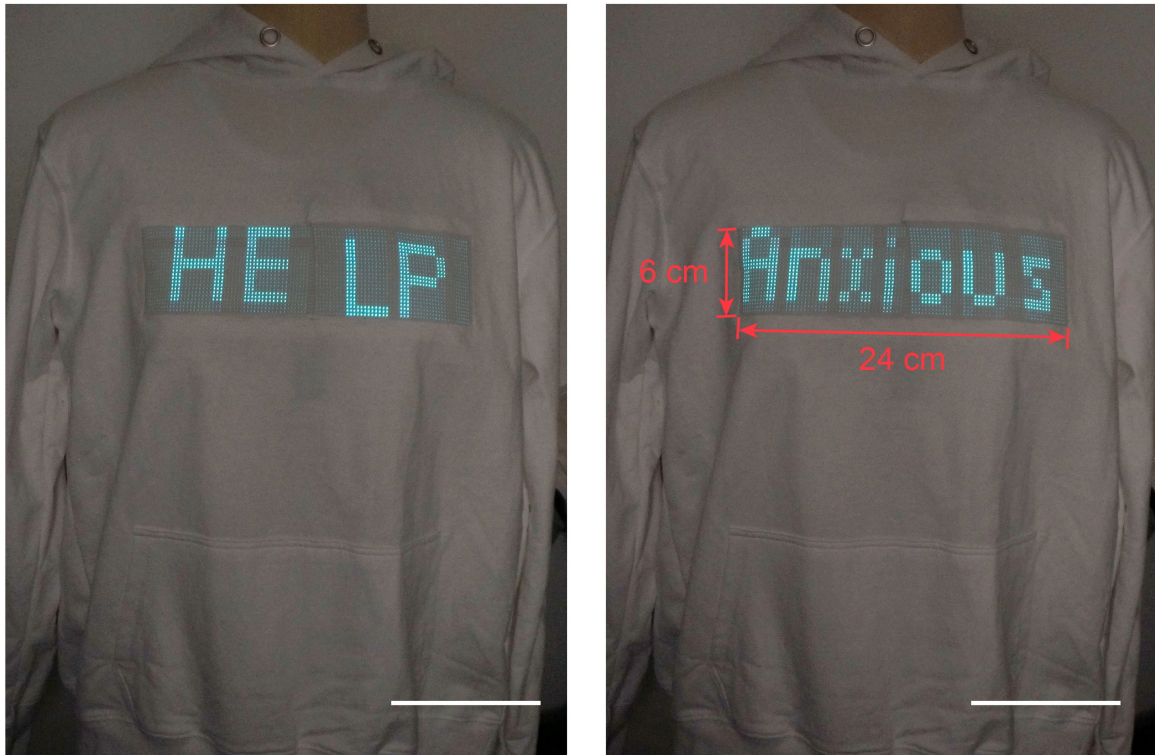
Extended Data Fig. 9 | Fabrication of the integrated textile system.

a, Schematic of the circuit design for the integrated textile system.

b, Photograph of an integrated textile system woven on a sleeve. Scale bar, 5 cm. **c**, Photograph shows conductive fibres serving as connecting lines are sewn into the textile using a digital sewing machine. Scale bar, 5 mm.


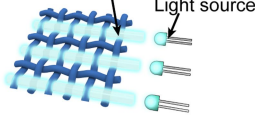
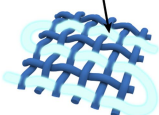
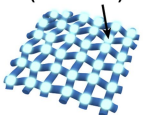
d, Photograph with outline showing the integrated circuit in the textile system. Scale bar, 5 cm.

e-g, Magnified views of the connecting lines sewn into the textile. Scale bars, 2 cm. **h, i**, Photographs show that the folded connecting points remain sturdy. Scale bars, 1 cm.



Extended Data Fig. 10 | A large display textile measuring 24 cm × 6 cm (length × width). Scale bars, 10 cm.

Extended Data Table 1 | Comparison of the current electroluminescent textile technologies

EL textile	Thin film ¹⁹ 	Optical fibre ²² 	EL fibre ²³⁻²⁶ 	EL unit (this work) 
Material	PET substrate, metal electrodes, conjugated organic semiconductors	PMMA or silica	metal wire, light-emitting polymer electrolyte/ ZnS phosphor	ZnS phosphor, polymer-based conductive fibre
Fabrication	vacuum deposition, spin coating	hot drawing	multilayer coating, twisting of fibre electrodes	weft-warp contacting
Working mode	pixel display	limitation to lighting of woven pattern through extra light sources	limitation to lighting of woven pattern	pixel display
Breathability	low	high	high	high
Flexibility	function degradation under high bending curvature in textile	rigid, brittle	flexible	flexible
Washing stability	N/A	N/A	N/A	stable

*PET, polyethylene terephthalate; PMMA, polymethyl methacrylate.
Refs. ^{19,22-26}.